Received: 26 September 2017 | Revised: 22 January 2018 | Accepted: 22 January 2018

DOI: 10.1002/mrm.27129

FULL PAPER

Magnetic Resonance in Medicine

Feasibility of in vivo measurement of glucose metabolism in the mouse hypothalamus by ^{1}H-[^{13}C] MRS at 14.1T

Blanca Lizarbe[1] | Hongxia Lei[2] | Joao M.N. Duarte[1] | Bernard Lanz[1,3] | Antoine Cherix[1] | Rolf Gruetter[1,2,4]

[1] Laboratory of Functional and Metabolic Imaging (LIFMET), École Polytechnique Fédérale de Lausanne, Lausanne, Switzerland

[2] Department of Radiology, University of Geneva, Geneva, Switzerland and Center for Biomedical Imaging (CIBM), Lausanne, Switzerland

[3] Sir Peter Mansfield Imaging Centre, School of Physics and Astronomy, University of Nottingham, Nottingham, United Kingdom

[4] Department of Radiology, University of Lausanne, Lausanne, Switzerland

Correspondence
Blanca Lizarbe, Laboratory for Functional and Metabolic Imaging (LIFMET), École Polytechnique Fédérale de Lausanne (EPFL). CH F1 612 (Bâtiment CH) Station 6, 1015 Lausanne, Switzerland.
Email: blanca.lizarbeserra@epfl.ch

Funding information
The work was supported by Center of Biomedical Imaging (CIBM) of the École Polytechnique Fédéral de Lausanne (EPFL), Université de Lausanne (UNIL), Univeriste de Genève (UNIGE), the Hôpitaux Univeristaires de Genève (HUG) and the Centre Hospitalier Universitaire Vaduois (CHUV), the Leenaards, Jeantet Foundations and Swiss National Science Foundation (149983). J. M.N.D. was supported by SNF Ambizione grant (148250)

Purpose: Determine the feasibility of ^{1}H-[^{13}C] MRS in the mouse hypothalamus using a 14.1T magnet.

Methods: We optimized the design of a ^{1}H-[^{13}C] surface coil to maximize the signal-to-noise ratio of ^{1}H-[^{13}C] MRS in the mouse hypothalamus. With enhanced signal, ^{13}C accumulation in glucose metabolites was measured in a 8.7 μL voxel in the hypothalamus of 5 healthy mice during the continuous administration of [1,6-$^{13}C_2$]glucose.

Results: Accumulation of ^{13}C label in glucose C6 and lactate C3 was visible in the hypothalamus 11 min after glucose administration. The ^{13}C fractional enrichment (FE) curves of lactate C3, glutamate and glutamine C4, glutamate+glutamine C3 and C2, GABA C2, C3, and C4, and aspartate C3 were measured with a time resolution of 11 min over 190 min. FE time-courses and metabolic pool sizes were averaged to fit a novel one-compartment model of brain energy metabolism that incorporates the main features of the hypothalamus.

Conclusion: Dynamic ^{1}H-[^{13}C] MRS is able to measure in vivo brain metabolism in small and deep areas of the mouse brain such as the hypothalamus, and it can be used to calculate metabolic fluxes, including glutamatergic and GABAergic metabolism as well as the contribution of metabolic sources other than glucose.

KEYWORDS
^{1}H-[^{13}C] MRS, glucose metabolism, hypothalamus

1 | INTRODUCTION

^{13}C MRS is a particularly versatile technique for noninvasively investigating brain metabolism. When used in combination with labeled substrates and high field magnets, the increased sensitivity of the technique can be used to explore small areas of the human and rat brain.[1,2] ^{13}C MRS experiments are typically performed while infusing [1-^{13}C]glucose, [1,6-$^{13}C_2$]glucose, or [2-^{13}C]acetate solutions into the blood and following their metabolism. During metabolic turnover, ^{13}C label is incorporated into various metabolites, and the more abundant ones are detectable by MRS. The label redistribution can be detected dynamically in vivo by ^{13}C MRS, and the application of appropriate mathematical models allows the calculation of metabolic fluxes.[3]

Compared with ^{1}H MRS, one of the major drawbacks of ^{13}C MRS is its lower sensitivity, which generally restricts its use to relatively large voxels placed close to a surface coil. Recent technological advances, however, such as increased magnetic field, improved shimming techniques, localization

methods, and RF coil designs have led to substantially greater sensitivity in *direct* and *indirect* ^{13}C MRS measurements.[4] For example, the surface coil arrangement designed by Adriany and Gruetter,[5] in which two ^{1}H loops were placed in quadrature and combined with a linearly polarized ^{13}C surface coil in between, enhanced detection sensitivity and enabled measurements in reduced volumes. With these improvements, both the rat and the mouse brain have been investigated using *direct* ^{13}C MRS.[6–8]

The hypothalamus is a small area deep inside the brain that senses energy metabolites, such as glucose, fatty acids, and ketone bodies, and hormones, such as leptin.[9–12] It contains different neuronal populations that participate in the short- and long-term regulation of energy balance,[13] and the neurotransmitters glutamate and γ-aminobutyrate (GABA) are present in most of its neurons.[14] The hypothalamus is a key regulator of glucose metabolism and insulin secretion,[15] and hypothalamic inflammation is implicated in the onset and development of obesity.[16] The establishment of a noninvasive approach to monitor hypothalamic metabolism could provide valuable new insights into the understanding of its normal function and in the longitudinal detection of any local changes during the course of a disease.

Earlier studies have used ^{1}H and ^{13}C MRS to investigate the hypothalamus, both in rodents and in humans,[17–21] and despite its small size and remote location in the brain, its neurochemical profile can be characterized in vivo.[22] ^{13}C MRS in vivo in the mouse hypothalamus has not been reported thus far, and the *direct* detection of ^{13}C label in such a small area distant from the RF coil would require the use of high magnetic field and maximized RF detection sensitivity to deliver sufficient signal. In this sense, *indirect* ^{1}H-[^{13}C] MRS detection methods, in which the ^{13}C label is quantified by evaluating the ^{13}C-induced heteronuclear coupling modifications on the ^{1}H resonances, can provide increased sensitivity, although at the expense of a lower spectral resolution.[23]

The aim of our study, therefore, was to detect ^{13}C turnover in the mouse hypothalamus in vivo by combining the use of high magnetic field with *indirect* ^{1}H-[^{13}C] MRS detection and a homemade surface coil optimized for this experiment. Furthermore, we calculated the local metabolic fluxes of the mouse hypothalamus by adapting the existing models of brain metabolism to include the metabolic activity of GABAergic neurons and any input from fatty acids and ketone bodies.[24,25]

2 | METHODS

2.1 | MR magnet and gradient coil

All measurements were carried out in a 14.1T magnet with a 26-cm-diameter horizontal bore (Magnex Scientific, Abingdon, UK), equipped with a 12-cm internal diameter gradient coil insert (400 mT/m, 120 μs), and interfaced to a DirectDrive console (Varian, Palo Alto, CA).

2.2 | RF coils

We used two different homemade transmit/receive surface coils: (1) the original ^{13}C-[^{1}H] surface coil used in Xin et al.[6] with two ^{1}H loops in quadrature (13 mm, 600 MHz) combined with a ^{13}C linearly polarized loop (11 mm, 150 MHz) placed in between them, and (2) an optimized ^{1}H-[^{13}C] coil with the ^{1}H (11 mm) loops placed below the ^{13}C loop (10 mm) (Figure 1). The optimized ^{1}H-[^{13}C] surface coil was designed specifically to enhance ^{1}H sensitivity in the hypothalamus by minimizing the distance between the ^{1}H loops and the mouse brain. Loop sizes were slightly modified to reach a reasonable compromise between geometrical decoupling (i.e., ≤-15 dB mutual coupling) and detection sensitivity, with the final coil arrangement yielding a geometrical coupling between the two ^{1}H loops of -20 dB, and ^{1}H-^{13}C coupling between the ^{13}C loop and each of the two ^{1}H loops of -16 dB and -24 dB, respectively. A glass sphere containing ^{13}C labeled formic acid (FA) was set at the center of the coils as a reference for ^{13}C frequency offset and ^{13}C channel power calibration.[26] In addition, to minimize crosstalk between the ^{1}H and ^{13}C transmission and reception lines during MRS experiments, proton- and carbon-bandpass filters were placed between the coil loops and the pre-amplifier.

2.3 | MR sequences

MR images were acquired with a fast spin echo (FSE) sequence and the following parameters: TE = 54 ms, repetition time = 4000 ms, echo train length = 8, averages = 4, slice thickness = 0.6 mm, slices = 15, field of view = 20 × 20 mm^2, data matrix = 256 × 256. The volumes of interest (VOIs) in vivo, were positioned based upon referencing the anatomical MR images to a mouse brain atlas.[27] For the in vitro acetate phantom tests, the VOIs were positioned with the same distance from the coil as in the in vivo experiments (5.1 mm below brain surface).

Field homogeneity was optimized by adjusting both first and second order shim gradients using FAST(EST)MAP methods.[28]

^{1}H-[^{13}C] MRS data were acquired with a full-intensity BISEP-SPECIAL sequence (BISEP: B_1-insensitive spectral editing pulse[29]; SPECIAL: SPin ECho, full Intensity Acquired Localized spectroscopy[30], with TE/TR = 2.8/4000 ms, 16 scans per block, and the ^{13}C inversion pulse alternating between OFF and ON in an interleaved mode.[29]

Optimization was performed for both the excitation and refocusing pulses in the SE localization sequence.[30] The durations and bandwidths were 2 ms/10 kHz for the spatially

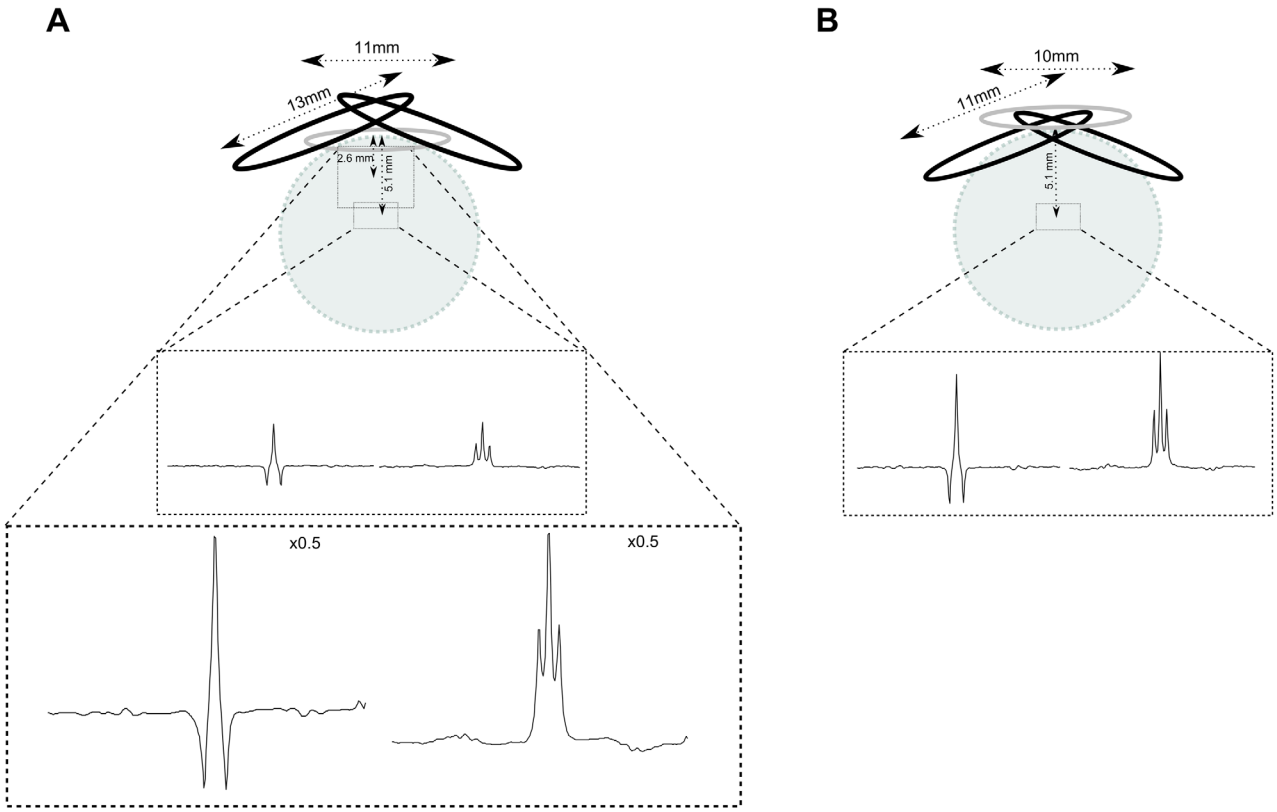

FIGURE 1 A, Schematic representation of the ^{13}C-[^{1}H] surface coil arrangement and the nondecoupled MRS spectra from the 50% labeled [2-^{13}C] acetate phantom. The two proton loops in quadrature (13 mm) were placed on top of the ^{13}C loop (11 mm). The big (5 mm × 4 mm × 3 mm) (top) and small hypothalamic (1.8 mm × 2.7 mm × 1.8 mm) (bottom) voxels were placed at 2.6 mm and 5.1 mm from the surface, respectively. The summed *inverted* and *non-inverted* spectra (12 averages each, line broadening = 20 Hz), from the top or bottom voxels, respectively, are plotted connected with the two respective volumes by dotted lines. The vertical scale of the big voxel spectra was modified (× 0.5) to smooth visualization. B, Schematic representation of the optimized ^{1}H-[^{13}C] surface coil and resulting MRS spectra from the 50% labeled [2-^{13}C]acetate phantom. The two proton loops in quadrature (11 mm) were located below the ^{13}C loop (10 mm) to maximize ^{1}H sensitivity of the mouse hypothalamus. The hypothalamic voxel (1.8 mm × 2.7 mm × 1.8 mm) was positioned at 5.1 mm from the phantom surface. The summed *inverted* and *non-inverted* spectra (12 averages each, line broadening = 20 Hz) are shown connected to the hypothalamic voxel

selective adiabatic inversion pulse, 0.5 ms/13.7 kHz for the excitation and 1 ms/6.7 kHz for refocusing. The resulting maximum chemical shift displacement errors were less than 8%, 6%, and 12%, respectively.

Localization of the VOI was improved with outer volume suppression.[31] For satisfactory water suppression, seven chemical shift-selective (CHESS) 15 ms RF pulses with variable power and optimized relaxation delays (VAPOR) were used, along with an additional 12-m Gaussian CHESS pulse between the spatially-selective inversion pulse and the excitation pulse.

In the BISEP module, the bandwidth of the inversion pulse of ^{1}H channel was ∼2 kHz (3.3 ppm at 14.1T) with γB_{1max} = 6.7 kHz, and the bandwidth of the inversion pulse of ^{13}C channel was 12 kHz (80 ppm at 14.1T) with γB_{2max} = 7 kHz.

Adiabatic ^{13}C decoupling (hyperbolic secant HS8 adiabatic full-passage pulse[32] together with a MLEV-4 cycle and five-step phase supercycle[33] was applied during the entire acquisition period (145 ms).

2.4 | Phantom setup

The quality of the ^{1}H-[^{13}C] MR hypothalamic signal was initially assessed on a phantom containing 50% enriched sodium [2-^{13}C]acetate (50 mM, Sigma-Aldrich, St. Louis, MO). First, SNRs of ^{1}H-[^{13}C] MR signals from two volumes: (1) a voxel mimicking the mouse hypothalamus size (1.8 mm × 2.7 mm × 1.8 mm) and depth (5.1 mm below brain surface) and (2) a voxel containing the mouse thalamus and cortex, analogous to that in Xin et al.[6] (5 mm × 4 mm × 3 mm), were compared using the original ^{13}C-[^{1}H] surface coil (Figure 1A). The SNR of ^{1}H-[^{13}C] MR signal from the identical voxel mimicking the mouse hypothalamus using the optimized ^{1}H-[^{13}C] surface coil was then determined (Figure 1B).

SNRs of six *inverted* and six *non-inverted* spectra (two averages each) were evaluated manually by dividing the maximum signal resonance intensity by the standard deviation of the baseline. The corresponding SNRs of the different voxels and coils were, respectively, averaged and compared (Figure 1).

In addition, RF powers for inversion and decoupling in the ^{13}C channel were calibrated for the different voxel distances to the coil (measured on the MRI using the FA bubble as landmark). The frequency offsets of the inversion pulses were centered at 1.81 ppm for the ^{1}H channel and 24.5 ppm for the ^{13}C channel, respectively. The ^{13}C decoupling module was centered at 24.5 ppm.

2.5 | Animal preparation

All experimental procedures involving animals were approved by the local ethics committee (EXPANIM-SCAV, Switzerland). Five adult (13 weeks old) male C57BL/6 mice were fasted overnight (12 h) before experiments. Body weight (29 ± 1 g) and fasting blood glucose levels (5.1 ± 1.3 mM) were measured at each experimental session. Isoflurane anesthesia (3-4% for induction, 2% for cannulation, 1-1.5% for maintenance, mixed with 1:1 air:O_2) was administrated through a nose cone and regulated to maintain a breathing rhythm between 70 and 100 breaths per min (SA Instruments, Stoney Brook, NY). Before the MR measurements, a femoral vein was cannulated for the infusion of a 20% mass per volume solution of [1,6-$^{13}C_2$]glucose (Sigma-Aldrich, St. Louis, MO). Then, animals were immobilized in a semi-cylindrical home-built holder with a bite bar and the head fixed with ear bars. Throughout the entire study, body temperature was monitored with a rectal probe (SA Instruments, Stoney Brook, NY) and maintained between 36.5 and 37.5 °C with a circulating water tube.

2.6 | ^{1}H-[^{13}C] MRS of the mouse hypothalamus

In the hypothalamus voxel, field homogeneity was optimized to a water linewidth of 16 ± 2 Hz. ^{13}C power values were chosen based on the measured voxel-to-coil distance and adjusted for coil loading (as compared to the phantom tests), using the FA flip angle optimization as a reference. The proton frequency offset of the inversion pulse was set to the resonance frequency of Glu C4 protons (2.34 ppm). The carbon frequency offset of the inversion pulse was set to 40 ppm to guarantee the complete inversion range between Glc C6 (62 ppm) and Lac C3 (21 ppm). The carrier frequency of the ^{13}C decoupling pulse was centered at 40 ppm.

After optimizing the ^{1}H-[^{13}C] sequence parameters for the dynamic ^{1}H-[^{13}C] MRS study of the mouse hypothalamus in vivo, the glucose solution was administered first as a 5-min bolus (4.01 mL/kg of 99% enriched ^{13}C glucose), followed by a constant infusion (10 mL/kg/h of 70% enriched ^{13}C glucose) for the rest of the experiment. The infusion rate was optimized to achieve a stable isotopic enrichment of plasma glucose.[34]

2.7 | Data analysis

For each animal, five consecutive *^{13}C-inverted* and *non-inverted* spectra, acquired in an interleaved mode, were frequency corrected and added together, resulting in two 80-scan blocks of *inverted* and *non-inverted* spectra. Each pair of 80 *inverted* and *non-inverted* spectra was subtracted to generate a ^{13}C-*edited* difference spectrum (160 scans) with an 11-min temporal resolution. Metabolite pool sizes were calculated from the *non-inverted* spectra using LCModel[35] and a standard basis set of metabolite spectra.[36,37] This basis set consists of simulations of 22 metabolites, including the macromolecules, alanine (Ala), aspartate (Asp), phosphorylcholine (PCho), creatine (Cr), phosphocreatine (PCr), GABA, glucose (Glc), glutamine (Gln), glutamate (Glu), glutathione, glycine, *myo*-inositol (Ins), lactate (Lac), N-acetylaspartate, *scyllo*-inositol, taurine, ascorbate, *N*-acetylaspartylglutamate, glycerylphosphorylcholine (GPC), phosphoethanolamine, and acetate, which can be used to define a neurochemical profile.

The intensities of the sum of Glu and Gln (Glx), the sum of GPC+PCho, and total Cr (Cr+PCr) were provided by LCModel. Cr+PCr values were used as an internal reference, assuming a total concentration of 8 μmol/g.[22,38] Quantification of the ^{13}C-*edited* spectra was done using another simulated basis set[6] that contains the resonances of ^{1}H coupled to NAA C6, Glu (C2, C3, and C4), Gln (C2, C3, and C4), GABA (C2, C3, and C4), Asp (C2 and C3), Glc (C1 and C6), Glx (C2 and C3), Lac C3, and Ala C3. Correlation values between the respective spectral intensities obtained with LCModel were controlled for every time point and animal. For some animals, GABA C3 and GABA C4 could not be detected in the first two time points, and its contribution was not taken into account. SNRs values of the both *edited* and *non-edited* spectra were obtained from LCModel.

Isotopic fractional enrichment (FE) values were calculated from the ratios between the *edited* and *non-edited* spectra, as described previously.[29] For example, FE values for Lac C3 were calculated at every time point by dividing the Lac C3 concentration obtained from the ^{13}C-*edited* spectra by total Lac values derived from the *non-edited* spectra analysis. ^{13}C concentrations were obtained by multiplying each FE by the corresponding metabolite pool size.

Glx C2 and Glc C6 FEs and ^{13}C concentrations were corrected to account for their respective correlated quantifications. These high correlations derive from their overlapping resonances in the ^{1}H spectrum, which occur between 3.88 and 3.71 ppm (Glc C6) and 3.76 and 3.75 ppm (Glx C2), and result in highly correlated signal intensities after LCModel-fitting. Adjustments were performed assuming three conditions: (1) no significant Glx C2 was labeled between $t = 0$ and $t = 11$ min, suggesting that (2) the measurement of Glc

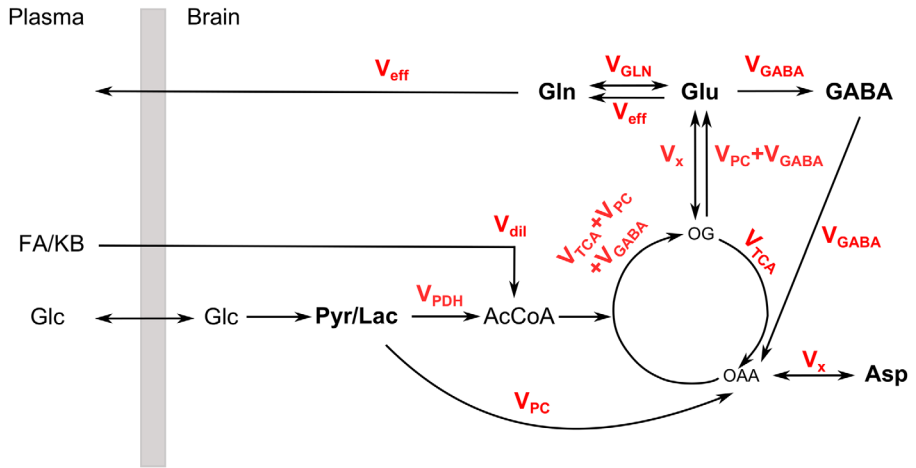

FIGURE 2 Schematic layout of the one-compartment model of hypothalamic metabolism. Labeled and nonlabeled glucose (Glc) enters the brain and is transformed into pyruvate (Pyr), which is in rapid exchange with lactate (Lac). Pyr is converted to acetyl-CoA (AcCoA) at a rate described by the pyruvate dehydrogenase flux ($\mathbf{V_{PDH}}$). Through an anaplerotic reaction, pyruvate carboxylase catalyzes the carboxylation of Pyr to form oxaloacetate (OAA) at rate $\mathbf{V_{PC}}$. Ketone bodies and fatty acids (FA/KB) can also enter the brain, and by an oxidative removal of successive two-carbon units in the form of acetyl-CoA, dilute AcCoA enrichment at rate $\mathbf{V_{dil}}$. AcCoA is further transformed to 2-oxoglutarate (OG) in the first turn of the TCA cycle, with a total consumption rate of $\mathbf{V_{PDH}+V_{dil}}$, equal to the sum of the oxidation fluxes $\mathbf{V_{PC}+V_{TCA}+V_{GABA}}$. $\mathbf{V_{TCA}}$ represents the rate of conversion from OG to OAA and $\mathbf{V_{GABA}}$ accounts for the GABA synthesis rate from Glu and for its further oxidation in the TCA cycle, originating OAA. OG exchanges labeling symmetrically with glutamate (Glu) by means of the transmitochondrial flux $\mathbf{V_x}$, while $\mathbf{V_{PC}}$ and $\mathbf{V_{GABA}}$ support a net conversion of OG to Glu. The Glu-Gln cycle is signified by a $\mathbf{V_{Gln}}$ exchange flux, and the loss of Gln is expressed by the $\mathbf{V_{eff}}$ flux, which is equal in value to the $\mathbf{V_{PC}}$ flux through mass-balance considerations assuming constant metabolites pool sizes (metabolic steady-state). OAA is modeled to exchange labeling with Asp through the transmitochondrial flux $\mathbf{V_x}$

C6 between t = 0 and t = 11 min was accurate, and (3) FE of Glc C6 was constant for the rest of the time course of the experiment ($FE_{Glc\ C6(t)}=FE_{Glc\ C6(t=6\ min)}$). Then, Glx C2 FEs were calculated using the expression:

$$FE_{Glx\ C2(t)}=({}^{13}C_{Glc\ C6(t)\ LCModel}+{}^{13}C_{Glx\ C2(t)\ LCModel}{}^{-1}H_{Glc\ t)\ LCModel}*FE_{Glc\ C6(t=6\ min)})/{}^{1}H_{Glx(t)\ LCModel}$$

where ${}^{13}C_{Glc\ C6(t)\ LCModel}$ and ${}^{13}C_{Glx\ C2(t)\ LCModel}$ represent the respective ^{13}C concentrations of Glc C6 and Glx C2 measured from the *edited* spectra, and ${}^{1}H_{Glx(t)LCModel}$ represents the total concentration of Glx measured from the *non-edited* spectra.[13]C concentrations were corrected accordingly.

Total pool sizes, FEs and ^{13}C concentrations were estimated for every time point. Curves of all animals were averaged and used for the metabolic flux analyses. Results are shown as mean ± SD values except otherwise stated.

2.8 | Modeling of hypothalamic metabolism

Hypothalamic metabolism was evaluated using a novel one-compartment model of brain metabolism (Figure 2) that retains the most relevant metabolic features of astrocytes, glutamatergic and GABAergic neurons by adapting a more complex three-compartment approach[39] to a single-TCA-cycle model. Additionally, it includes the net contribution of fatty acids and ketone bodies as non-labeled energy substrates to hypothalamic metabolism.[40–42] The metabolic model was applied to fit average FE turnover curves of Glu C4, Gln C4, GABA C2, GABA C3, GABA C4, Glx C3, Glx C2, and Asp C3 and using average metabolic pool sizes. Time resolution was set to 11 min, except for Asp C3, where it was increased to 18 min to reach similar SNR. The Lac C3 curve, measured in the hypothalamus in vivo, was used as the input function.[6]

Fitting was performed in MATLAB (Version 8.2, The MathWorks, Inc., Natick, MA). Values of the metabolic rates of the pyruvate dehydrogenase complex (V_{PDH}), the tricarboxylic acid cycle (V_{TCA}), the dilution flux (V_{dil}), the pyruvate carboxylase (V_{PC}), the glutamate-GABA cycle (V_{GABA}), the glutamate-glutamine cycle (V_{Gln}), the transmitochondrial flux (V_x), the efflux flux (V_{eff}), and their respective uncertainties were calculated by a two-step method. First, the fluxes were estimated using the FE curves weighted by the inverse of their variance (based on their respective noise level), with a standard built-in ordinary differential equation solver and a modified Levenberg-Marquardt nonlinear weighted regression method.[6] Subsequently, precision of the metabolic rates was determined by 300 Monte Carlo simulations of the FE time courses. The SD provided by their respective fittings was used to define the rates' uncertainties.[3] Correlation values between fluxes were calculated during the nonlinear regression algorithm. The resulting simulated FE turnover curves of all measured ^{13}C resonances, obtained with values from the best fit of the metabolic fluxes, were compared with the corresponding experimental curves to evaluate the accuracy of the modeling. All corresponding

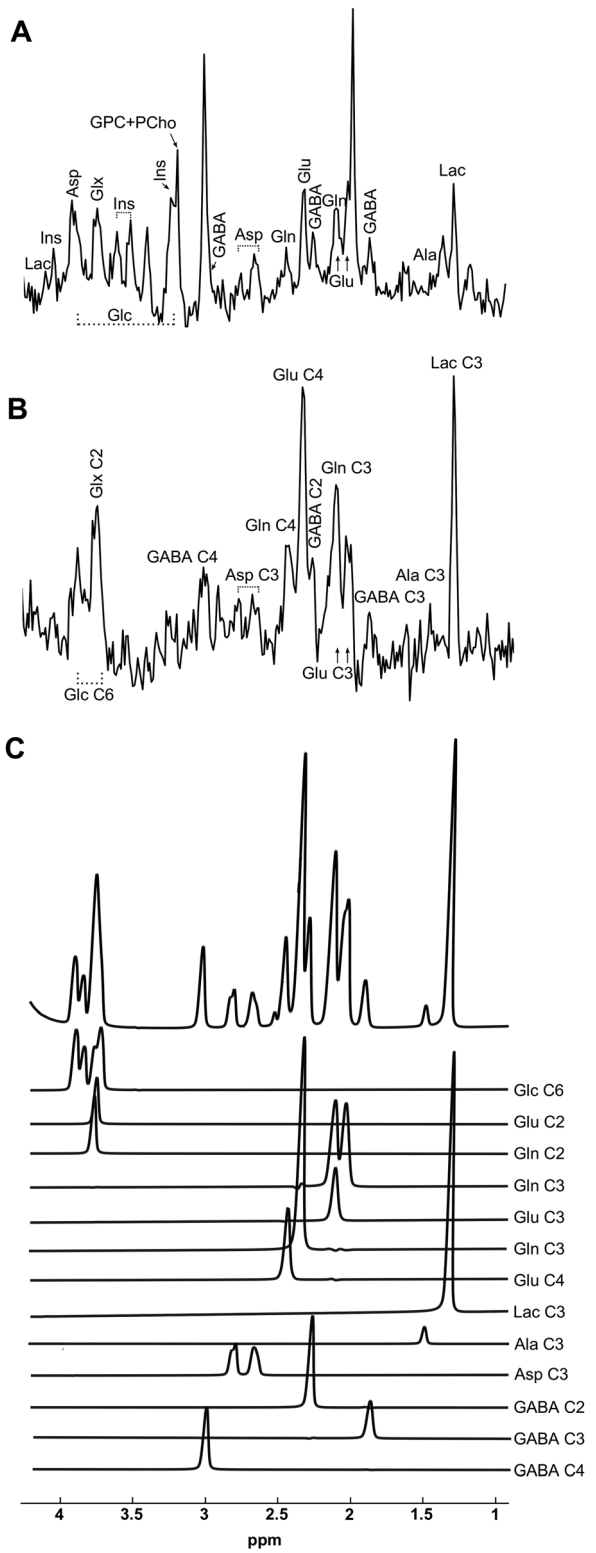

FIGURE 3 A, Typical *non-edited* spectrum (80 scans, 5.3 min with the acquisition distributed in 11 min) of the mouse hypothalamus after 150 min of continuous Glc infusion. B, ^{13}C-*edited* spectrum (160 scans, 11 min) of the same animal and time point. C, LCModel-fit of the ^{13}C-edited spectrum and individual fit of Glc C6, Glu (C2, C3 and C4), Gln (C2, C3 and C4), Lac C3, Ala C3, Asp C3, and GABA (C2, C3, and C4). The vertical scale of the edited spectrum (line broadening = 5 Hz) is 3 times lower than the scale in the *non-edited* spectrum

mass-balance and differential equations of the mathematical model are provided in Supporting Information, which is available online.

To evaluate the effect of small variations of the Glc C6 and Glx C2 FEs values on the metabolic rates, two data sets with either a 10% artificially-increased $FE_{Glc\ C6\ (t=6min)}$ values or with a 10% decrease were generated and fitted to the one-compartment model. The resulting metabolic rates were compared with the original results by permutation analysis followed by Student's t-tests, as detailed previously.[43]

3 | RESULTS

3.1 | ^{1}H-[^{13}C] MRS coil tests on a [2-^{13}C] acetate phantom

To evaluate the modified RF coil design, both coils were tested on the phantom containing 50% labeled [2-^{13}C]acetate. Using the original ^{13}C-[^{1}H] coil, the resulting *inverted* and *non-inverted* spectra from the big voxel exhibited equally high quality, and their corresponding SNRs were not different from each other, i.e., 127.8 ± 7.5 and 126.3 ± 8.0 ($P > 0.05$), respectively (Figure 1A, bottom). SNRs of *inverted* and *non-inverted* spectra from the hypothalamic voxel under the identical settings were substantially reduced, i.e., 30.5 ± 2.2 and 30.4 ± 2.3, respectively (Figure 1A, top). Tests with the optimized ^{1}H-[^{13}C] coil yielded hypothalamic *inverted* and *non-inverted* spectra with improved quality and SNRs of 90.8 ± 5.0 and 91.5 ± 3.3, respectively.

3.2 | ^{1}H-[^{13}C] MRS of the mouse hypothalamus at 14.1T

The metabolite linewidths of the *non-edited* spectra from the mouse hypothalamus were 16 ± 2 Hz, and SNRs were 14 ± 1, as measured with LCModel (Figure 3A). Neurochemical quantification revealed high levels of GABA (3.83 ± 0.08 μmol/g) (mean ± SEM between all animals), Ins (7.38 ± 0.16 μmol/g), and total choline (GPC+PCho, 2.05 ± 0.04 μmol/g), and low levels of Ala (0.8 ± 0.04 μmol/g). In addition, Glc (2.73 ± 0.19 μmol/g), Glu (8.98 ± 0.30 μmol/g), Gln (3.51 ± 0.14 μmol/g), Lac (3.81 ± 0.15 μmol/g), and Asp (2.26 ± 0.08 μmol/g) were quantified. Glc concentration increased throughout the study, reaching a final level of 6.61 ± 1.0 μmol/g. The remaining metabolites had stable concentrations, except Lac, which decreased to a final concentration of 2.82 ± 0.6 μmol/g.

In the *edited* spectra, ^{13}C-coupled ^{1}H resonances of Lac C3, Ala C3, GABA C3, Glx C3, GABA C2, Glu C4, Gln C4, Asp C3, GABA C4, Glx C2, and Glc C6 were clearly visible in an 11-min scan, 150 min after the beginning of the infusion (Figure 3B).

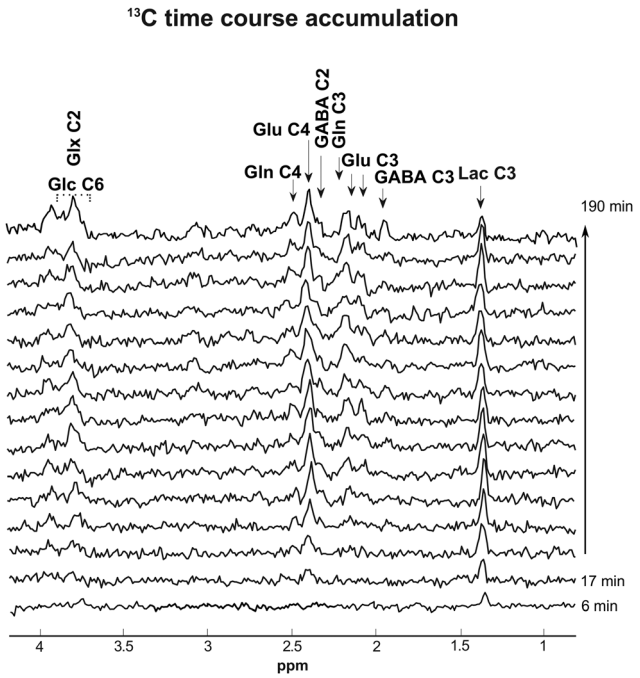

FIGURE 4 Stack of ^{1}H-[^{13}C] *edited* spectra (line broadening = 5 Hz) showing one time course (190 min) accumulation of labeling in a single animal

During the first 11 min of acquisition, the presence of Glc C6 and Lac C3 resonances in the ^{13}C-*edited* spectra was revealed (Figure 4). ^{13}C-coupled ^{1}H resonances of Glu C4 and Gln C4 appeared in the second time-point spectrum, and GABA C2, Glx C3 became perceptible from the 3rd *edited* spectrum.

SNRs of *edited* spectra increased along the time course. For all the mice, at the first time point measurement, SNR was approximately 2, as measured with LCModel, while in the last time point it was around 4. Mean CRLBs of the ^{13}C-coupled resonances of all time points were 15 ± 5% for Glc C6, 6 ± 5% for Glu C4, 17 ± 10% for Gln C4, 7 ± 1% for Lac C3, 18 ± 11% for GABA C2, 24 ± 19% for GABA C3, 11 ± 10% for Glx C3, and 18 ± 7% for Glx C2. Concentrations for Asp C3 were obtained from the 18 min time resolution spectra, and the average CRLB was 32 ± 8%. Quantification of Ala C3 was only possible from approimately 150 min of glucose infusion and not in all animals. Correlation of spectral intensities derived from LCModel fitting (Figure 3C) generally resulted in a very small value except for Glu C3 with Gln C3, Glu C2 with Gln C2, and between Glx C2 and Glc C6, where absolute correlation values were around -0.8 for almost all time points. These high correlations precluded the use of Glu C3 and Gln C3 and Glu C2 and Gln C2 independently. Therefore, Glx C2 and C3 were used instead.

FEs curves were obtained for Lac C3, Glu C4, Gln C4, GABA (C2, C3 and C4), Glx C3, Glx C2, and Asp C3 (Figure 5).

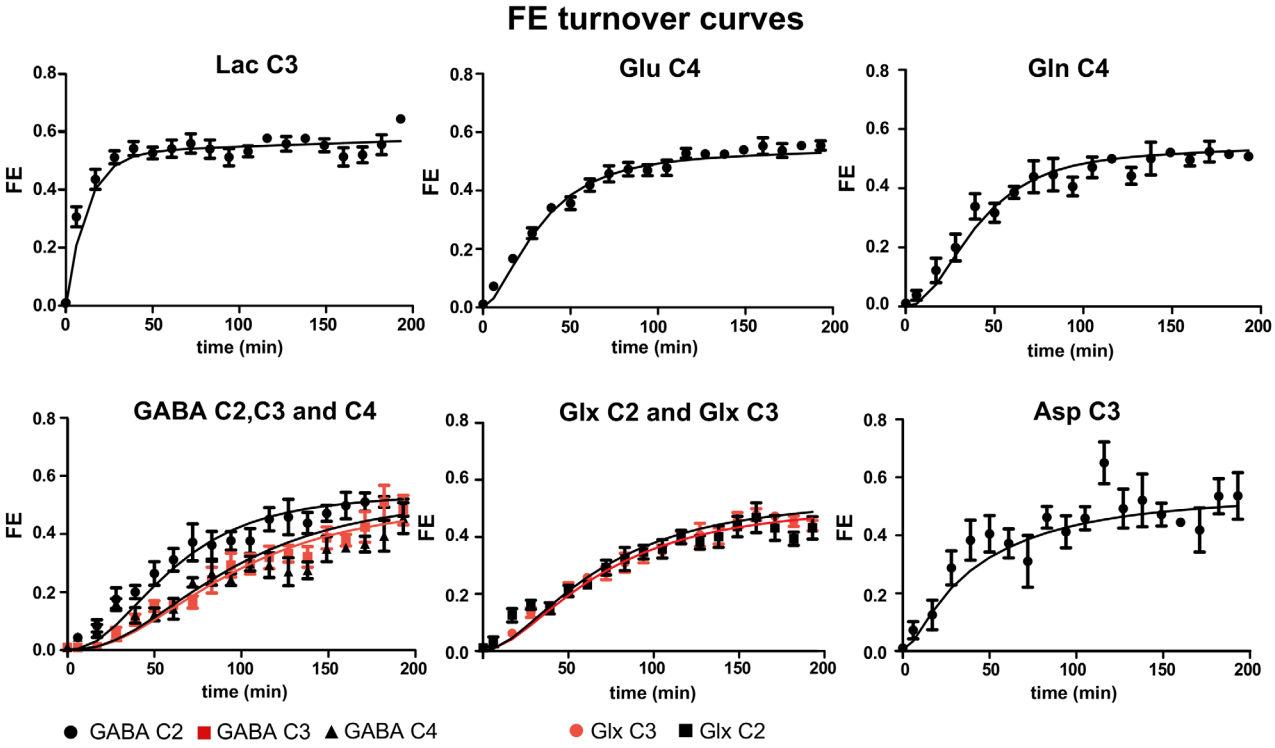

FIGURE 5 Mean (±SEM) turnover curves of the FE of lactate C3 (Lac C3), glutamate C4 (Glu C4), glutamine C4 (Gln C4), GABA C2, C3 and C4, glutamate C3 + glutamine C3 (Glx C3), glutamate C2 + glutamine C2 (Glx C2), and aspartate C3 (Asp C3). Lines in Lac C3 FE curves depict the respective fitting of the data to the step function $f(t)=(a\cdot t+b)\cdot\left(1-exp(-c\cdot t)\right)$ and lines in Glu C4, Gln C4, GABA C2, C3, and C4, Glx C3, Glx C2, and Asp C3 show the fit of the data to the one-compartment metabolic model

The fractional enrichment of Lac C3 rose rapidly, reaching a plateau enrichment of 0.53 ± 0.09. As for Glu C4 and Gln C4, their ^{13}C concentrations reached steady-state values of 5.03 ± 0.08 μmol/g and 1.89 ± 0.40 μmol/g, respectively, after approximately 130 min of glucose infusion (FE of 0.55 ± 0.03 and 0.50 ± 0.06, respectively). GABA C2 values reached a plateau of 1.63 ± 0.47 μmol/g at 150 min (FE = 0.49 ± 0.06), GABA C3 reached a stable concentration of 1.60 ± 0.09 μmol/g toward the end of the measurements and GABA C4 1.51 ± 0.15 μmol/g (FE of 0.47 ± 0.11 and 0.45 ± 0.10, respectively). Glx C3 and Glx C2 reached steady-state values of 5.65 ± 0.48 μmol/g and 5.55 ± 0.11 μmol/g at approximately 150 min (FE of 0.44 ± 0.04 and 0.43 ± 0.08, respectively). Asp C3 reached a steady-state of 1.00 ± 0.22 μmol/g (FE = 0.49 ± 0.10) after approximately 90 min.

3.3 | Mathematical modeling of hypothalamic metabolism

Fitting of the mathematical model of hypothalamic metabolism to the FEs turnover curves yielded a TCA flux V_{TCA} of 0.83 ± 0.05 μmol/g/min, a transmitochondrial flux V_x of 0.68 ± 0.21 μmol/g/min, a neurotransmitter Glu-Gln flux V_{Gln} of 0.41 ± 0.07 μmol/g/min, a Glu-GABA flux V_{GABA} of 0.13 ± 0.01 μmol/g/min, a dilution flux V_{dil} of 0.06 ± 0.01 μmol/g/min and a V_{PC} of 0.04 ± 0.01 μmol/g/min. Using the calculated V_{TCA}, V_{GABA}, V_{PC}, and V_{dil} fluxes, the pyruvate dehydrogenase rate V_{PDH} and total rate of mitochondrial oxidation ($V_{PDH}+V_{dil}$) were determined, resulting in a V_{PDH} of 0.94 ± 0.05 μmol/g/min and $V_{PDH}+V_{dil}$ of 1.01 ± 0.05 μmol/g/min. Fluxes were used to generate FE simulated values that are in excellent agreement with the experimental data (Figure 5). Correlation values between fluxes were generally <0.4 and the highest correlation was between V_{GABA} and V_{TCA} (-0.4). Modeling of the artificially augmented or decreased Glc C6 FEs yielded values of the metabolic rates that were not significantly different ($P > 0.05$) from the original results.

4 | DISCUSSION

The present study reports for the first time the feasibility to obtain metabolic fluxes of the mouse hypothalamus noninvasively using dynamic *indirect* ^{1}H-[^{13}C] MRS at 14T. The particular challenges of dynamic ^{13}C MRS on the mouse hypothalamus were overcome by two approaches: (1) using proton detection methods with labeled [1,6-$^{13}C_2$]glucose and (2) maximizing the sensitivity of ^{1}H detection with an optimized surface coil geometry. Additionally, a new one-compartment model that encompasses the main metabolic characteristics of the hypothalamus is proposed.

The optimized coil arrangement generated SNRs of the hypothalamic spectra from the [2-^{13}C]acetate phantom (~90) that were substantially enhanced, e.g., 3 times higher, as compared to the SNR from the identical voxel settings using the original ^{13}C-[^{1}H] coil configuration (~30), and only 30% less than the SNR from the large voxel with the nonoptimized geometry (~130). Hence, the SNRs of the hypothalamic *edited* spectra in vivo over 11 min were comparable to that obtained from a 60 μL volume with a 5-min time resolution during dynamic ^{13}C MRS in the mouse cortex.[6]

The use of [1,6-$^{13}C_2$]glucose infusion in this study provided two unique advantages over the widely used [1-^{13}C]glucose and [U-^{13}C]glucose substrates. First, it increased the ^{13}C labeling by two-fold, compared with [1-^{13}C]glucose. Second, it required less RF power for the adiabatic pulses than is needed for [U-^{13}C]glucose. [1,6-$^{13}C_2$]Glucose-derived signals require narrower inversion and decoupling RF bandwidths, i.e., 40 ppm (from Lac C3 to Glc C6), compared with 60 ppm for [U-^{13}C]glucose signals (from Lac C3 to Glc C2-5). With narrower bandwidths, adiabatic pulses require less RF power. Using [1,6-$^{13}C_2$]glucose, however, we observed high correlations between the Glc C6 and Glx C2 fitted signal intensities, due to their overlapping resonances (3.88-3.71 ppm, 3.76 ppm and 3.75 ppm for Glc, Gln, and Glu, respectively) (Figure 3C). To correct for these correlations, and based on the design of the glucose infusion protocol,[34] we used a constant FE for Glc C6, measured in the first time point.

This assumption resulted in approximately equivalent calculated steady-state FEs of Glx C2 and Glx C3, as noted in previous studies.[43] Moreover, small artificial variations of the glucose enrichment (±10%) did not significantly affect the calculated metabolic flux values. Glx C2-Glc C6 correlations could be avoided using [U-^{13}C]glucose, but reliable quantification of the Glc C2-C5 positions would require the use of substantially higher RF power for the inversion and decoupling. The geometrical configuration of our optimized coil, with the proton loops closer to the brain surface, results in a greater ^{13}C loop-hypothalamus distance, compared with the original configuration, and required the use of higher inversion and decoupling RF power on the ^{13}C channel. In this sense, the correct quantification of the [U-^{13}C]glucose-derived Glc C2-C5 signals might have resulted in needing to use RF power exceeding the coil limits. Moreover, with [U-^{13}C]glucose, the incorporation of Ala C2 resonance (at 3.78 ppm) would need to be taken into account.

The average FE turnover curves from the mouse hypothalamus were fitted to a modified one-compartment model of brain metabolism that includes two of the main features of hypothalamic metabolism, namely the abundant GABAergic neurons and the potential contributions of energy sources other than glucose.[44] In our model, the total rate of mitochondrial oxidation (1.01 ± 0.05 μmol/g/min) was very similar to the

whole mouse brain TCA cycle rate (1.05 ± 0.04 μmol/g/min) reported by Xin et al.[6] and slightly higher than the value reported by Lai et al.[45] (0.76 ± 0.04 μmol/g/min). In the aforementioned studies, however, no net contribution of nonlabeled substrates was considered, while our results indicate a 6% contribution of fatty acids or ketone bodies to the total mitochondrial oxidation rate.

Although it is small, this value refers explicitly to the net uptake of nonlabeled sources at the level of acetyl-CoA, and, if the fatty acid or ketone body contribution to hypothalamic metabolism changed, as it does in pathological conditions,[46–50] this change should become measurable. Within the total rate of oxidation reported here, 82% can be attributed to the TCA rate, 13% to GABAergic recycling and approximately 4% to V_{PC}. This represents a higher hypothalamic GABAergic metabolism than that reported in rats (9%)[39] and a very similar V_{PC} contribution than that previously reported in mice (5%).[45] The V_{GABA} flux fitted in our study (0.13 ± 0.01 μmol/g/min) is very similar to the GABAergic neurotransmitter cycling flux (0.11 ± 0.01 μmol/g/min) measured in the rat brain in vivo[39] and estimated in the mouse thalamic-hypothalamic area from brain extracts,[17] and it accounts for approximately 24% of the total neurotransmitter flux, similar to the 22% and 23% contributions described in the rat brain.[39,51]

The transmitochondrial (0.68 ± 0.21 μmol/g/min) and Glu-Gln rates (0.41 ± 0.07 μmol/g/min) are slightly higher in the hypothalamus than previously reported in rodents,[6,7,29] which can be related to the fact that glutamate underlies the majority of fast synaptic activity in this area.[52] However, when comparing these results to previous investigations using two- or three-compartment models, it should be noted that, because our model does not include separate cellular compartments, the neurotransmitter fluxes described here are simplifications of the more complex models, which take into account neurotransmitter cycling between compartments.

The excellent agreement between the fit and the experimental data reflects the suitability of the hypothalamic metabolic model proposed here. Specifically, the good agreement between the fitted GABA C2, C3, and C4 FE values with the experimental concentrations suggests that the simplified model can be used to determine the role of GABAergic neurons in hypothalamic metabolism.

Despite the narrow linewidths achieved in this study, Glu C3 resonances were strongly correlated with Gln C3, and likewise Glu C2 with Gln C2, due to the spectral overlap that persists even at 14.1T. This strong correlation limited the number of amino acids labeling positions and, therefore, precluded the extension of the modeling to a full two- or three-compartment model of neurotransmitter metabolism.[39,53] Such models could potentially improve the determination of the V_{dil} flux, especially because it has been suggested that fatty acids and ketone bodies are mostly taken up by astrocytes.[42,54,55]

We conclude that in vivo ^{1}H-[^{13}C] MRS is feasible in the mouse hypothalamus despite its very small size and distance from the surface coil. The application of ^{13}C MRS to such small volumes opens the possibility of studying the mouse brain metabolism in vivo in the hypothalamus and other areas with specific physiological or pathological conditions.

ACKNOWLEDGMENTS

The authors acknowledge Dr. L. Xin for providing very valuable help during quantification of the *inverted* and *non-inverted* spectra and are indebted to Dr. H. Yoshihara for his exhaustive revision of the manuscript. The work was supported by Center of Biomedical Imaging (CIBM) of the École Polytechnique Fédéral de Lausanne (EPFL), Université de Lausanne (UNIL), Univeriste de Genève (UNIGE), the Hõpitaux Univeristaires de Genève (HUG) and the Centre Hospitalier Universitaire Vaduois (CHUV), the Leenaards, Jeantet Foundations and Swiss National Science Foundation (149983). JMND was supported by SNF Ambizione grant (148250).

ORCID

Blanca Lizarbe http://orcid.org/0000-0002-5531-4088

REFERENCES

[1] Pfeuffer J, Tkác I, Choi IY, et al. Localized in vivo 1H NMR detection of neurotransmitter labeling in rat brain during infusion of [1-13C] D-glucose. *Magn Reson Med.* 1999;41:1077-1083.

[2] Gruetter R, Adriany G, Choi IY, Henry PG, Lei H, Oz G. Localized in vivo 13C NMR spectroscopy of the brain. *NMR Biomed.* 2003;16:313-338.

[3] Lanz B, Gruetter R, Duarte JM. Metabolic flux and compartmentation analysis in the brain in vivo. *Front Endocrinol.* 2013;4:156.

[4] Lai M, Gruetter R, Lanz B. Progress towards in vivo brain 13C-MRS in mice: metabolic flux analysis in small tissue volumes. *Anal Biochem.* 2017;529:229-244.

[5] Adriany G, Gruetter R. A half-volume coil for efficient proton decoupling in humans at 4 Tesla. *J Magn Reson.* 1997;125:178-184.

[6] Xin L, Lanz B, Lei H, Gruetter R. Assessment of metabolic fluxes in the mouse brain in vivo using 1H-[13C] NMR spectroscopy at 14.1 Tesla. *J Cereb Blood Flow Metab.* 2015;35:759-765.

[7] Duarte JM, Lanz B, Gruetter R. Compartmentalized cerebral metabolism of [1,6-(13)C]glucose determined by in vivo (13)C NMR spectroscopy at 14.1 T. *Front Neuroenergetics.* 2011;3:3.

[8] Nabuurs CI, Klomp DW, Veltien A, Kan HE, Heerschap A. Localized sensitivity enhanced in vivo C-13 MRS to detect glucose metabolism in the mouse brain. *Magn Reson Med.* 2008;59:626-630.

[9] Lam TK, Schwartz GJ, Rossetti L. Hypothalamic sensing of fatty acids. *Nat Neurosci.* 2005;8:579-584.

[10] Hawkins RA, Biebuyck JF. Ketone-bodies are selectively used by individual brain-regions. *Science.* 1979;205:325-327.

[11] Karnani M, Burdakov D. Multiple hypothalamic circuits sense and regulate glucose levels. *Am J Physiol Regul Integr Comp Physiol.* 2011;300:R47-R55.

[12] Sahu A. Leptin signaling in the hypothalamus: emphasis on energy homeostasis and leptin resistance. *Front Neuroendocrinol.* 2003;24:225-253.

[13] Morton GJ, Cummings DE, Baskin DG, Barsh GS, Schwartz MW. Central nervous system control of food intake and body weight. *Nature.* 2006;443:289-295.

[14] Schoene C, Burdakov D. Glutamate and GABA as rapid effectors of hypothalamic "peptidergic" neurons. *Front Behav Neurosci.* 2012;6:81.

[15] Osundiji MA, Lam DD, Shaw J, et al. Brain glucose sensors play a significant role in the regulation of pancreatic glucose-stimulated insulin secretion. *Diabetes.* 2012;61:321-328.

[16] Thaler JP, Yi CX, Schur EA, et al. Obesity is associated with hypothalamic injury in rodents and humans. *J Clin Invest.* 2012; 122:153-162.

[17] Tiwari V, Ambadipudi S, Patel AB. Glutamatergic and GABAergic TCA cycle and neurotransmitter cycling fluxes in different regions of mouse brain. *J Cereb Blood Flow Metab.* 2013;33:1523-1531.

[18] Moheet A, Emir UE, Terpstra M, et al. Initial experience with seven tesla magnetic resonance spectroscopy of hypothalamic GABA during hyperinsulinemic euglycemia and hypoglycemia in healthy humans. *Magn Reson Med.* 2014;71: 12-18.

[19] Just N, Cudalbu C, Lei H, Gruetter R. Effect of manganese chloride on the neurochemical profile of the rat hypothalamus. *J Cereb Blood Flow Metab.* 2011;31:2324-2333.

[20] Violante IR, Anastasovska J, Sanchez-Canon GJ, et al. Cerebral activation by fasting induces lactate accumulation in the hypothalamus. *Magn Reson Med.* 2009;62:279-283.

[21] Delgado TC, Violante IR, Nieto-Charques L, Cerdan S. Neuroglial metabolic compartmentation underlying leptin deficiency in the obese ob/ob mice as detected by magnetic resonance imaging and spectroscopy methods. *J Cereb Blood Flow Metab.* 2011;31: 2257-2266.

[22] Lei H, Poitry-Yamate C, Preitner F, Thorens B, Gruetter R. Neurochemical profile of the mouse hypothalamus using in vivo 1H MRS at 14.1T. *NMR Biomed.* 2010;23:578-583.

[23] de Graaf RA, Rothman DL, Behar KL. State of the art direct 13C and indirect 1H-[13C] NMR spectroscopy in vivo. A practical guide. *NMR Biomed.* 2011;24:958-972.

[24] Morris AA. Cerebral ketone body metabolism. *J Inherit Metab Dis.* 2005;28:109-121.

[25] Hofmann K, Lamberz C, Piotrowitz K, et al. Tanycytes and a differential fatty acid metabolism in the hypothalamus. *Glia.* 2017;65:231-249.

[26] Gruetter R, Adriany G, Merkle H, Andersen PM. Broadband decoupled, H-1-localized C-13 MRS of the human brain at 4 Tesla. *Magn Reson Med.* 1996;36:659-664.

[27] Franklin KBJ, Paxinos G. *The Mouse Brain in Stereotaxic Coordinates*. Amsterdam: Academic Press; 2008.

[28] Gruetter R, Tkac I. Field mapping without reference scan using asymmetric echo-planar techniques. *Magn Reson Med.* 2000;43: 319-323.

[29] Xin L, Mlynarik V, Lanz B, Frenkel H, Gruetter R. 1H-[13C] NMR spectroscopy of the rat brain during infusion of [2-13C] acetate at 14.1 T. *Magn Reson Med.* 2010;64:334-340.

[30] Mlynarik V, Gambarota G, Frenkel H, Gruetter R. Localized short-echo-time proton MR spectroscopy with full signal-intensity acquisition. *Magn Reson Med.* 2006;56:965-970.

[31] Tkac I, Oz G, Adriany G, Ugurbil K, Gruetter R. In vivo 1H NMR spectroscopy of the human brain at high magnetic fields: metabolite quantification at 4T vs. 7T. *Magn Reson Med.* 2009; 62:868-879.

[32] Tannus A, Garwood M. Improved performance of frequency-swept pulses using offset-independent adiabaticity. *J Magn Reson A.* 1996;120:133-137.

[33] Fujiwara T, Anai T, Kurihara N, Nagayama K. Frequency-switched composite pulses for decoupling C-13 spins over ultrabroad bandwidths. *J Magn Reson A.* 1993;104:103-105.

[34] Henry PG, Lebon V, Vaufrey F, Brouillet E, Hantraye P, Bloch G. Decreased TCA cycle rate in the rat brain after acute 3-NP treatment measured by in vivo 1H-[13C] NMR spectroscopy. *J Neurochem.* 2002;82:857-866.

[35] Provencher SW. Automatic quantitation of localized in vivo 1H spectra with LCModel. *NMR Biomed.* 2011;14:260-264.

[36] Xin L, Gambarota G, Mlynarik V, Gruetter R. Proton T2 relaxation time of J-coupled cerebral metabolites in rat brain at 9.4 T. *NMR Biomed.* 2008;21:396-401.

[37] Kunz N, Cudalbu C, Mlynarik V, Hüppi PS, Sizonenko SV, Gruetter R, et al. Diffusion-weighted spectroscopy: a novel approach to determine macromolecule resonances in short-echo time 1H-MRS. *Magn Reson Med.* 2010;64:939-946.

[38] Tkác I, Henry PG, Andersen P, Keene CD, Low WC, Gruetter R. Highly resolved in vivo 1H NMR spectroscopy of the mouse brain at 9.4 T. *Magn Reson Med.* 2004;52:478-484.

[39] Duarte JM, Gruetter R. Glutamatergic and GABAergic energy metabolism measured in the rat brain by C-13 NMR spectroscopy at 14.1 T. *J Neurochem.* 2013;126:579-590.

[40] Frost G, Sleeth ML, Sahuri-Arisoylu M, et al. The short-chain fatty acid acetate reduces appetite via a central homeostatic mechanism. *Nat Commun.* 2014;5:3611.

[41] Melo TM, Nehlig A, Sonnewald U. Neuronal-glial interactions in rats fed a ketogenic diet. *Neurochem Int.* 2006;48:498-507.

[42] Blazquez C, Sanchez C, Velasco G, Guzman M. Role of carnitine palmitoyltransferase I in the control of ketogenesis in primary cultures of rat astrocytes. *J Neurochem.* 1998;71:1597-1606.

[43] Sonnay S, Duarte JM, Just N, Gruetter R. Compartmentalised energy metabolism supporting glutamatergic neurotransmission in response to increased activity in the rat cerebral cortex: a 13C MRS study in vivo at 14.1 T. *J Cereb Blood Flow Metab.* 2016; 36:928-940.

[44] Delgado TC. Glutamate and GABA in appetite regulation. *Front Endocrinol.* 2013;4:103.

[45] Lai M, Lanz B, Poitry-Yamate C, et al. In vivo (13)C MRS in the mouse brain at 14.1 Tesla and metabolic flux quantification

under infusion of [1,6-(13)C2]glucose. *J Cereb Blood Flow Metab.* 2017. https://doi.org/10.1177/0271678X17734101.

[46] Karmi A, Iozzo P, Viljanen A, et al. Increased brain fatty acid uptake in metabolic syndrome. *Diabetes.* 2010;59:2171-2177.

[47] Le Foll C, Levin BE. Fatty acid-induced astrocyte ketone production and the control of food intake. *Am J Physiol Regul Integr Comp Physiol.* 2016;310:R1186-1192.

[48] Lin AL, Zhang W, Gao X, Watts L. Caloric restriction increases ketone bodies metabolism and preserves blood flow in aging brain. *Neurobiol Aging.* 2015;36:2296-2303.

[49] Longo VD, Mattson MP. Fasting: molecular mechanisms and clinical applications. *Cell Metab* 2014;19:181-192.

[50] Roy M, Beauvieux MC, Naulin J, et al. Rapid adaptation of rat brain and liver metabolism to a ketogenic diet: an integrated study using (1)H- and (13)C-NMR spectroscopy. *J Cereb Blood Flow Metab.* 2015;35:1154-1162.

[51] Patel AB, de Graaf RA, Mason GF, Rothman DL, Shulman RG, Behar KL. The contribution of GABA to glutamate/glutamine cycling and energy metabolism in the rat cortex in vivo. *Proc Natl Acad Sci U S A.* 2005;102:5588-5593.

[52] van den Pol AN. Weighing the role of hypothalamic feeding neurotransmitters. *Neuron* 2003;40:1059-1061.

[53] Gruetter R, Seaquist ER, Ugurbil K. A mathematical model of compartmentalized neurotransmitter metabolism in the human brain. *Am J Physiol Endocrinol Metab.* 2001;281: E100-E112.

[54] Ebert D, Haller RG, Walton ME. Energy contribution of octanoate to intact rat brain metabolism measured by 13C nuclear magnetic resonance spectroscopy. *J Neurosci.* 2003;23:5928-5935.

[55] Auestad N, Korsak RA, Morrow JW, Edmond J. Fatty acid oxidation and ketogenesis by astrocytes in primary culture. *J Neurochem.* 1999;56:1376-1386.

SUPPORTING INFORMATION

Additional Supporting Information may be found in the supporting information tab for this article.

How to cite this article: Lizarbe B, Lei H, Duarte JMN, Lanz B, Cherix A, Gruetter R. Feasibility of in vivo measurement of glucose metabolism in the mouse hypothalamus by ^{1}H-[^{13}C] MRS at 14.1T. *Magn Reson Med.* 2018;80:874–884. https://doi.org/10.1002/mrm.27129